Engineering Structures 296 (2023) 116941

Contents lists available at ScienceDirect

Engineering Structures

journal homepage: www.elsevier.com/locate/engstruct

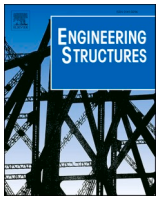

Cross-laminated timber (CLT) floor serviceability under multi-person loading: Impact of beam–panel connections

Junhui Zhang [a], Cong Zhang [a], Yi Li [a], Wen-Shao Chang [b,*], Haoyu Huang [c,*]

[a] Faculty of Architecture, Civil and Transportation Engineering, Beijing University of Technology, Beijing 100124, China
[b] Lincoln School of Architecture and the Built Environment, University of Lincoln, Lincoln LN6 7TS, UK
[c] School of Engineering, Newcastle University, Newcastle Upon Tyne NE1 7RU, UK

ARTICLE INFO

Keywords:
Floor vibration
Human-induced vibration
Comfort
Steel–timber connection
Screwed connection

ABSTRACT

Due to the lightweight nature of timber, vibration serviceability is a crucial issue in the design of timber floors. The purpose of this study is to investigate how beam–panel connections affect the vibration serviceability of cross-laminated timber (CLT) floors subjected to multi-person loading. Cyclic tests were carried out to determine the mechanical behaviour of steel beam–CLT panel connections with various screws sizes (diameters and lengths). A numerical model of a CLT floor was developed to determine the response to human-induced vibrations with different screw configurations (sizes and spacing). The results showed that the dynamic characteristics of the floor were slightly impacted by the screw size. However, as the spacing between screws reduced, the fundamental natural frequency increased by 4.3% and the vibration dose value (VDV) of the floor decreased by 38.3%. A theoretical model was introduced to predict the fundamental natural frequency of a CLT floor system. In addition, a design method for predicting the vibration serviceability, in terms of VDV, of low-frequency CLT floors was proposed.

1. Introduction

The construction sector accounts for almost 40% of global CO_2 emissions [1]. Construction with renewable resources plays a significant role in achieving sustainable development goals [1,2]. Timber structures have been gaining popularity worldwide as an innovative solution to reduce CO_2 emissions and sequester atmospheric carbon [3]. The demand for timber constructions is steadily rising across the globe. Nearly 1700 mass timber projects were in design or constructed in the US by December 2022 [4], and over 300,000 timber floors are constructed annually in the UK [5]. However, given the lightweight nature of timber, timber floors are vulnerable to excessive vibration, especially in modern buildings designed with open spaces for flexible use [6]. For lightweight floors, the design must consider the serviceability limit state, which typically entails deflection and vibration check to prevent discomfort instead of the ultimate limit states [7].

Vibration serviceability standards and guidelines include several authoritative sources, such as EN 1995–1-1 (Eurocode 5) [8], ISO 10137 [9], BS 6472-1 [10], SCI P354 [11], JRC–ECCS Joint Report (JRC 55118) [7], AISC Design Guide 11 [12], and CCIP 016 [13]. Researchers aim to improve the vibration serviceability of timber floors and have conducted extensive studies on evaluation criteria and design approaches for floors. To minimise floor vibrations, Ellingwood and Tallin [14] reviewed and proposed tentative serviceability criteria. Using design methods, Smith and Chui [15] predicted the dynamic behaviour of lightweight wood-joist floors covered with wood-based sheathings. Arshad et al. [16] presented dynamic-based design curves that related root-mean-square acceleration to floor fundamental frequency to evaluate timber floors exposed to normal human activities. Onysko et al. [17] reviewed the aspects of serviceability design of timber-framed residential floors in Canada. Hu et al. [18] chronologically reviewed the development of design approaches to minimise excessive vibrations in residential timber floors. Hu and Chui [19] developed a vibration-controlled criterion and a calculation method for determining criterion parameters. Hamm et al. [20] developed rules and suggestions for the design and construction of timber floors without vibration problems based on measurements of real buildings and in the laboratory. Weckendorf et al. [21] contributed to the resolution of the debate regarding the control of floor response characteristics by design methods. Chang et al. [5] proposed a design method for timber floors not covered by Eurocode 5.

Timber floor vibration is not only influenced by floor properties

* Corresponding authors.
E-mail addresses: wchang@lincoln.ac.uk (W.-S. Chang), haoyu.huang@newcastle.ac.uk (H. Huang).

https://doi.org/10.1016/j.engstruct.2023.116941
Received 25 April 2023; Received in revised form 22 August 2023; Accepted 21 September 2023
Available online 28 September 2023

(such as aspect ratio [22]) but also boundary conditions. In study [23], it was observed that modifying the arrangement of supporting beams has a significant impact on the dynamic properties and vibration response of cross-laminated timber (CLT) floors. The connection between the floor and the support was also found to influence the frequency and damping ratio of timber floors. For instance, in study [24], by changing the floating floors to screwed floors, the fundamental natural frequency increased from 11.0 Hz to 12.8 Hz, and the damping ratios increased from 2.2% to 2.6% accordingly. In another study [25], researchers conducted shear tests on connections and vibration tests on full-scale floors to examine the vibration performance of CLT–glulam composite floors. However, they found limited variations in fundamental natural frequencies when altering the CLT–glulam connections. While literature has focused on the boundary conditions of CLT floors, no specific research has investigated the influence of steel beam–CLT panel connections on floor vibration serviceability. The steel–timber hybrid construction system, which combines a steel frame with timber panels, has gained attention as a promising structural form [26–29]. To further advance the use of CLT in the building industry, it is essential to investigate the influence of steel beam–CLT panel connections on the vibration serviceability of floors.

Screw-type fasteners can be feasibly used to connect timber panels to the steel frame because they can transfer the interface shear and develop composite action between the timber and steel by bearing and mobilising friction resistance [26,27,30]. Coach screws are commonly used in steel–timber connections [31]. Previous studies have conducted investigations, including bending tests, static push-out tests, and low-cycle high amplitude cyclic loading tests on steel–CLT connections [30,32–34] and static push-out tests on steel–laminated veneer lumber connections [35]. However, the above studies only focused on the performance of connections themselves and disregarded the vibration serviceability of floors. Recent studies have investigated the vibration behaviour of CLT floors using different types of connectors [25,36,37]. However, limited sizes of a few types of screws were involved, for example, only coach screws with the diameter of 12 and 16 mm were investigated. In addition, these studies evaluated the vibration serviceability using the maximum deflection and maximum velocity method, peak acceleration method, and OS-RMS90-value method. The vibration dose value (VDV) method was not used. As introduced in BS 6472-1 [10], the VDV method can take into account the factors that affect occupants' acceptance of vibration such as distribution of vibration amplitude, how often the vibration of a particular level occurs, and how long the occupant is exposed to the vibration. Hence, it has been widely used to comprehensively assess different types of vibrations, such as continuous, intermittent, and impulsive vibrations. None have specifically investigated the influence of coach screws on the vibration serviceability of CLT floors by VDV.

This paper aims to investigate the effect of coach-screwed steel beam–CLT panel connections on the vibration serviceability of CLT floors. The key parameters are the size (diameter and length) of and spacing between coach screws. Cyclic tests were first conducted on specimens of beam–panel connections with various screw sizes. Then, the results were used to establish and verify a numerical model of a full-scale CLT floor, referring to the experimental results of the previous research [22]. The vibration performance of floors with different screw configurations was analysed, and a theoretical model that considered beam–panel connections was proposed to estimate the fundamental natural frequency of the CLT floor. Finally, a design method for predicting the vibration serviceability (in terms of VDV) of low-frequency CLT floors was proposed.

2. Cyclic tests of steel beam–CLT panel connection

Under human-induced excitation, the response of the steel beam–CLT panel floor system can be divided into the bending of the panel and rotation of the boundary. Specifically, the rotation of the boundary can be further subdivided into the torsion of the beam and the shear of the beam–panel connection. Fig. 1 illustrates the situation for a CLT panel supported by two steel beams. In this section, shear tests were conducted on connection specimens fastened by coach screws. The connections were subjected to cyclic loading under tension and compression, and their deformation modes and load–displacement responses were obtained.

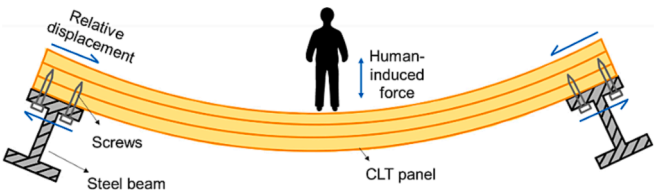

Fig. 1. Deformation of steel beam–CLT floor.

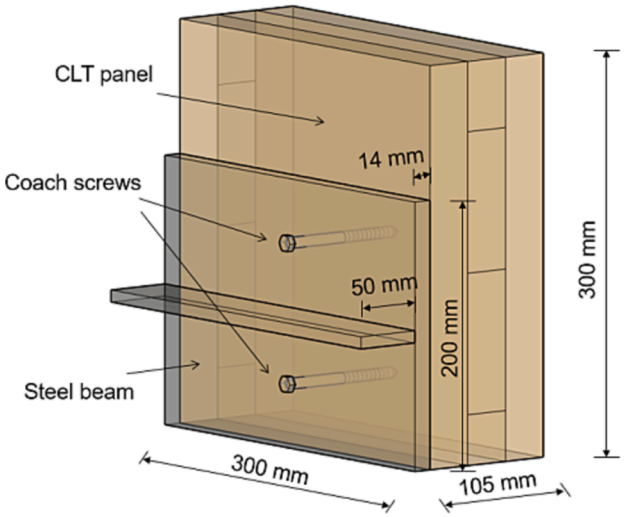

Fig. 2. Dimensions and details of steel–CLT connection.

2.1. Experiment study

2.1.1. Materials

This study utilised three-ply CLT specimens with a total thickness of 105 mm (layup: 35L-35T-35L) and 300 mm length and width. The specimens were manufactured by Ningbo Sino-Canada Low-Carbon Technology Research Institute Co. Ltd., using hemlock spruce with a density of approximately 500 kg/m^3. The modulus of elasticity parallel to the grain was 10767 MPa, and that perpendicular to the grain was 979 MPa. Meanwhile, the embedment strength was around 25 MPa. The mechanical properties were obtained from the manufacturer and documented in the product testing report. The report was based on laboratory tests using the exact same batch of CLT used in this study. The average moisture content during the tests was 12%.

To facilitate the tests, steel plates were assembled to represent the

Fig. 3. Coach screws used in cyclic tests.

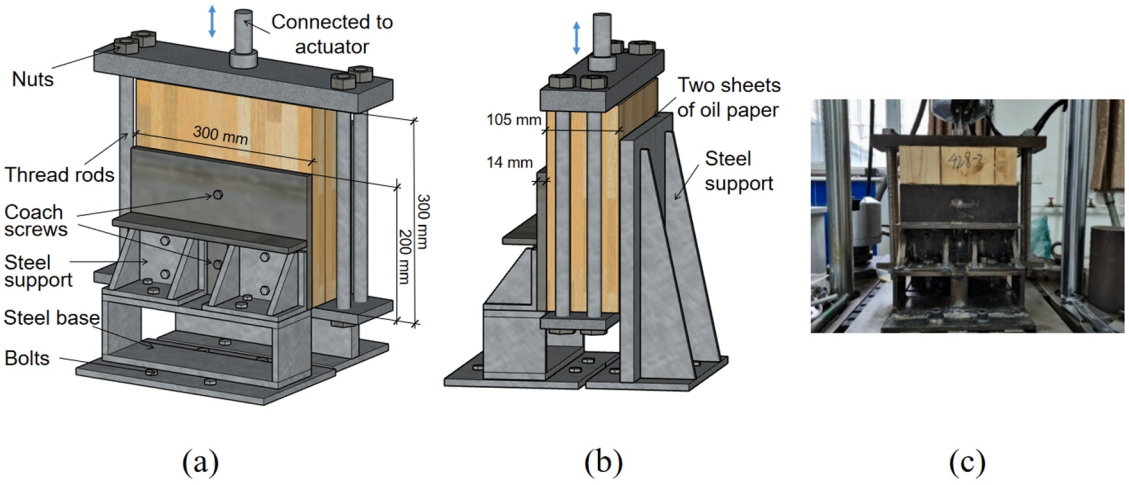

Fig. 4. Schematic of a specimen from (a) left front view and (b) left rear view; and (c) a specimen mounted on the machine.

top flange and a part of the steel beam web (Fig. 2). The steel beam used was HN 450 × 200 (specified in GB/T 11263-2017 [38]), with a section depth of 450 mm, a 14 mm-thick and 200 mm-width flange and a 9 mm-thick web. The steel beam was 300 mm in length, equivalent to the CLT panel's length. The steel used was Q235 steel, as specified in the GB/T 700-2006 [39].

Hexagon head coach screws, also known as lag screws, were used in this study, as specified in DIN 571 [40]. Nine screw sizes, covering diameters of 6, 8, and 10 mm and lengths of 60, 80, and 100 mm, were selected. In this paper, the screws sizes are presented in the format of 'M screw diameter (nominal size) × screw length (mm)' (Fig. 3).

2.1.2. Test set-up

In this section, a specimen was designed to simulate a three-ply CLT floor placed on the top flange of a steel beam. The CLT panel and the steel beam were connected using coach screws (Fig. 2). To facilitate the installation of coach screws, predrilled holes were fabricated on the steel beam with an additional 0.2 mm allowance to avoid tight-fitting of the screws with the steel plate [33]. According to Eurocode 5 [8], the diameter of predrilled holes on the CLT panels should not exceed the inner thread diameters of the coach screws. Therefore, the diameters of predrilled holes on the CLT panel for M6, M8, and M10 screws were set as 4, 6, and 8 mm, respectively, in this study.

Fig. 4(a) and 4(b) show the left front and left rear views of the specimen, respectively, and Fig. 4(c) shows the specimen mounted on the testing machine. To ensure that the steel beam remained in place throughout the tests, the flange was connected to the steel base using steel supports and the base was firmly fixed to the testing machine with bolts. The CLT panel was fastened by tightly clamping the upper and lower steel plates through threaded rods and nuts. The testing machine applied a vertical load to the CLT panel by controlling the actuator connecting to the upper steel plate. Given that the steel beam had a fixed location during the tests, the relative displacement between the CLT panel and steel beam was determined from the recorded displacement of the actuator. Extra steel support was placed behind the CLT panel to restrict its horizontal movement. In addition, two sheets of oil packing paper were used to minimise friction between the CLT panel and the steel support. The loading direction was parallel to the grain of the outer layer of the CLT panel, same as previous research by Wang et al. [22]. A low-cycle fatigue loading machine was used for the cyclic tests. The machine had a maximum load capacity of ± 50 kN and an actuator stroke of 50 mm. The machine recorded the force at the beam–panel connection and the relative displacement between the beam and CLT panel.

Table 1
Test protocol.

Test No.	Diameter of the screw (mm)	Length of the screw (mm)
1	6	60
2		80
3		100
4	8	60
5		80
6		100
7	10	60
8		80
9		100

2.1.3. Test procedure

A total of 27 specimens were subjected to displacement-controlled loading in accordance with the loading protocol illustrated in Fig. 5. Investigation was conducted on 9 different screw sizes, with 3 replicates performed for each screw size to ensure the reliability of results. All the 27 specimens were produced using the same batch of CLT as used in

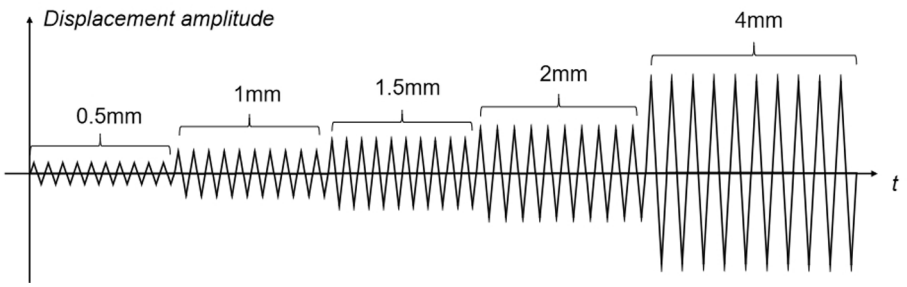

Fig. 5. Loading protocol for cyclic test.

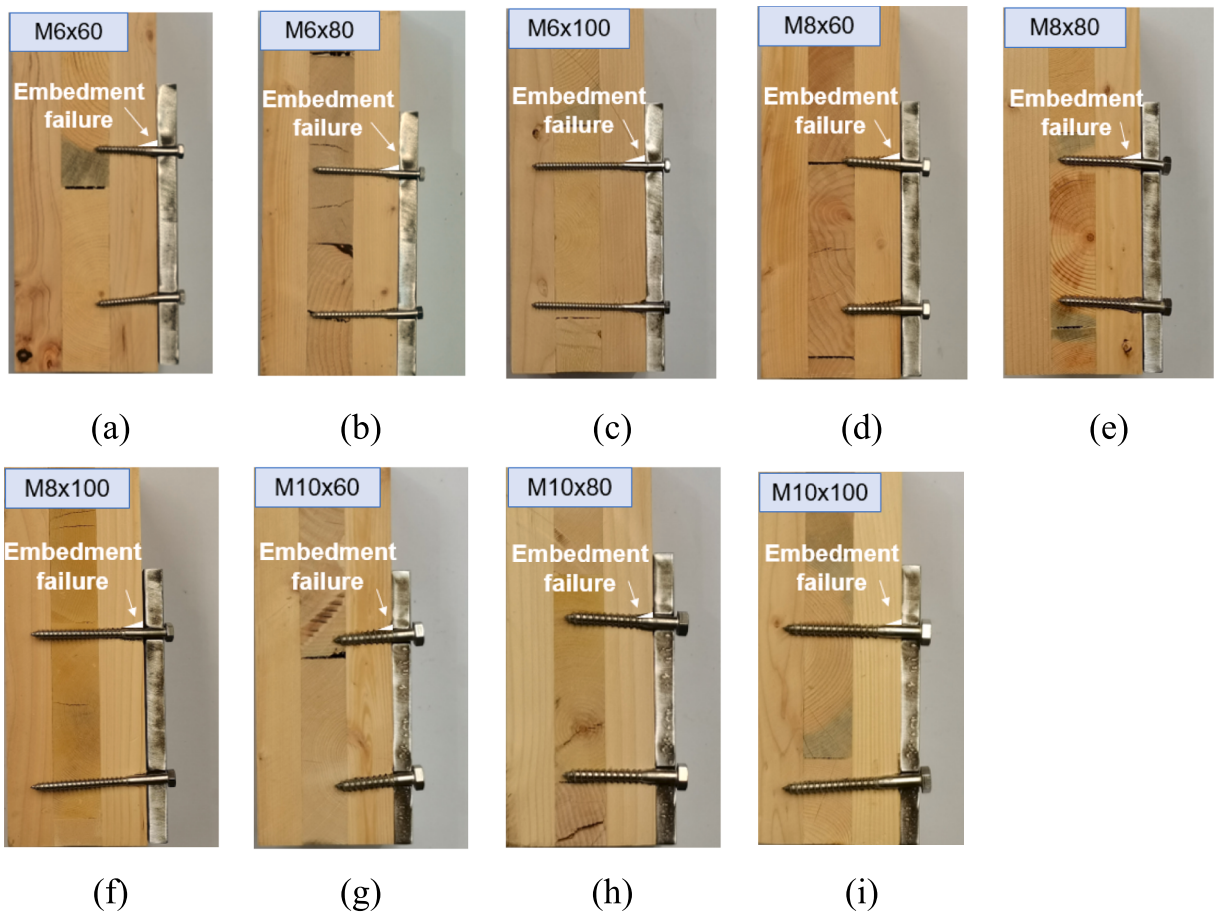

Fig. 6. Deformation modes of (a) M6 × 60, (b) M6 × 80, (c) M6 × 100, (d) M8 × 60, (e) M8 × 80, (f) M8 × 100, (g) M10 × 60, (h) M10 × 80, and (i) M10 × 100.

previous research [22]. The test protocol is presented in Table 1. In a pilot study, a three-ply CLT panel placed on two steel beams without connectors was simulated in OpenSees and subjected to multi-person loading. The results showed that the relative displacement between the steel beam and the CLT panel along the longitudinal direction of the floor reached and remained stable at around 4 mm. Therefore, it is assumed that the maximum relative displacement between the steel beam and the CLT panel is 4 mm and the maximum displacement amplitude applied in this study was set to 4 mm. The amplitudes were set at 0.5, 1, 1.5, 2, and 4 mm in sequence, and ten cycles were performed for each amplitude to investigate the damping decay of the connection, following the methodology of a previous study [41]. A loading frequency of 4 Hz was selected for the cyclic tests in this study. In previous research [22], it was found that the floor exhibited vibration that closely matched its fundamental natural frequency of approximately 5 Hz when a footfall excitation at a slow walking pace (around 1 Hz) was applied. In addition, according to BS 6472–1:2008 [10], individuals are most sensitive to vertical vibration within the frequency range of 4 to 12.5 Hz. Considering the aforementioned factors and taking into account the limitations of the testing machine (with a maximum capacity of 4 Hz), the loading frequency of the tests was set to be 4 Hz. The test method outlined in EN 12512 [42] was not performed in this study, because it is typically used to determine the complete load–displacement envelop curve (i.e. the slip increases progressively until failure, or a slip of 30 mm is reached) or to obtain the main characteristics at pre-determined ductility. However, in this study, the floor under human-induced excitation did not reach failure, and no pre-determined ductility requirement was applied.

2.2. Experimental results and discussion

2.2.1. Deformation modes

Although previous research has focused on the failure modes of steel–timber connections [8], this study aimed to investigate the deformation modes and serviceability performance of these connections. Fig. 6 presents the cross-sectional views of the beam–panel connections using various sizes of screws.

No obvious deformation was observed at the flange of the steel beam after the cyclic tests. However, in all specimens, embedment failure of the outer layer of the CLT occurred in the vicinity of the screws, and this finding can be attributed to the low elastic modulus of CLT and localised strain near the penetrations [35]. This study focused on the vibration serviceability of floors, and as such, the cyclic loading applied during the tests was not intended to cause specimen failure.

2.2.2. Load-displacement behaviour

Fig. 7 displays the load–displacement behaviour of specimens with different screw sizes. The data presented in the figure represent the performance of one of the three replicates for each screw size. The selected specimens exhibited performances that were similar to the average of the replicates, and the following analysis was based on these specimens. As depicted in Fig. 7, the hysteretic curves exhibited 'pinching', a typical phenomenon for timber connections with dowel-type fasteners [43]. Specifically, the load did not increase significantly until the displacement approached the maximum displacement achieved during previous load cycles [44]. The pinching phenomenon is attributable to the enlargement of the original hole in the CLT occupied by the screw [45]. During the cyclic test, the screw resisted the CLT, which caused irrecoverable embedment deformations. This pinching

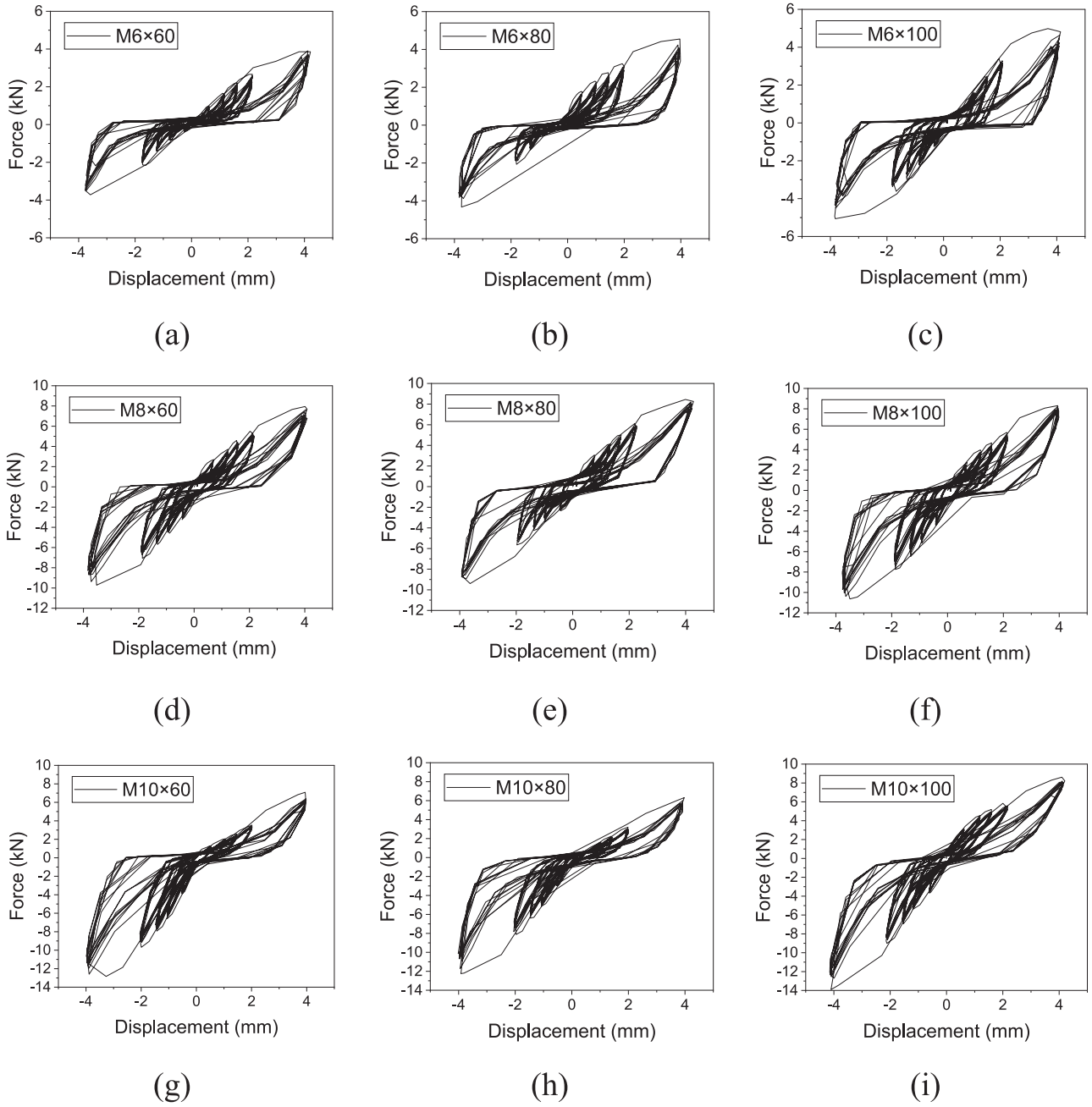

Fig. 7. Hysteretic curves corresponding to (a) M6 × 60, (b) M6 × 80, (c) M6 × 100, (d) M8 × 60 mm, (e) M8 × 80, (f) M8 × 100, (g) M10 × 60, (h) M10 × 80, and (i) M10 × 100 screw.

phenomenon was observed at all loading amplitudes, with more pronounced effects observed as the amplitudes increased.

2.2.3. Damping capacity

The damping performance of connections is crucial for energy dissipation in timber structures [41]. One common way to quantify hysteresis damping properties is through the use of equivalent viscous damping ratio (EVDR). According to EN 12512:2001 [42], EVDR is given by Eq. (1):

$$EVDR = E_d/(2\pi E_p) \tag{1}$$

where E_d is the energy dissipated per half cycle of load–displacement response, and E_p is the available potential energy (Fig. 8(a)). In several cases in this study, an imbalance was observed between tension and compression. Thus, Eq. (1) was modified to Eq. (2):

$$EVDR = E_{d,c}/(2\pi E_{p,c}) \tag{2}$$

where $E_{d,c}$ is the energy dissipated in a complete cycle of load–displacement response, and $E_{p,c}$ is the available potential energy corresponding to a complete cycle.

To depict the energy dissipation of each specimen, the EVDR of the 1st and 10th cycles of the load–displacement response at each amplitude was calculated according to Eq. (2), and the results are shown in Fig. 9. The dissipation of energy in a steel beam–CLT panel connection is mainly influenced by three factors, including screw deformation, timber compression caused by the screw, and friction between the timber panel and beam flange [23,46]. Fig. 9 illustrates that there is no significant correlation between the EVDR and screw sizes. This lack of correlation

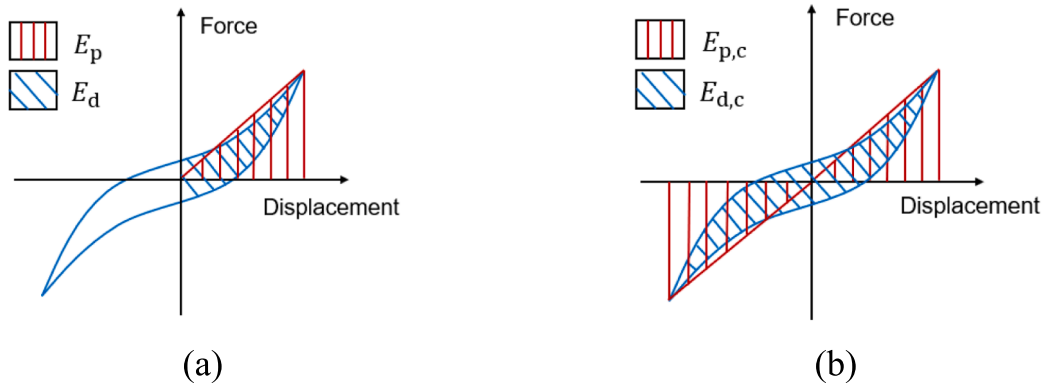

Fig. 8. Hysteretic area for EVDR calculation in (a) EN 12512 and (b) this study.

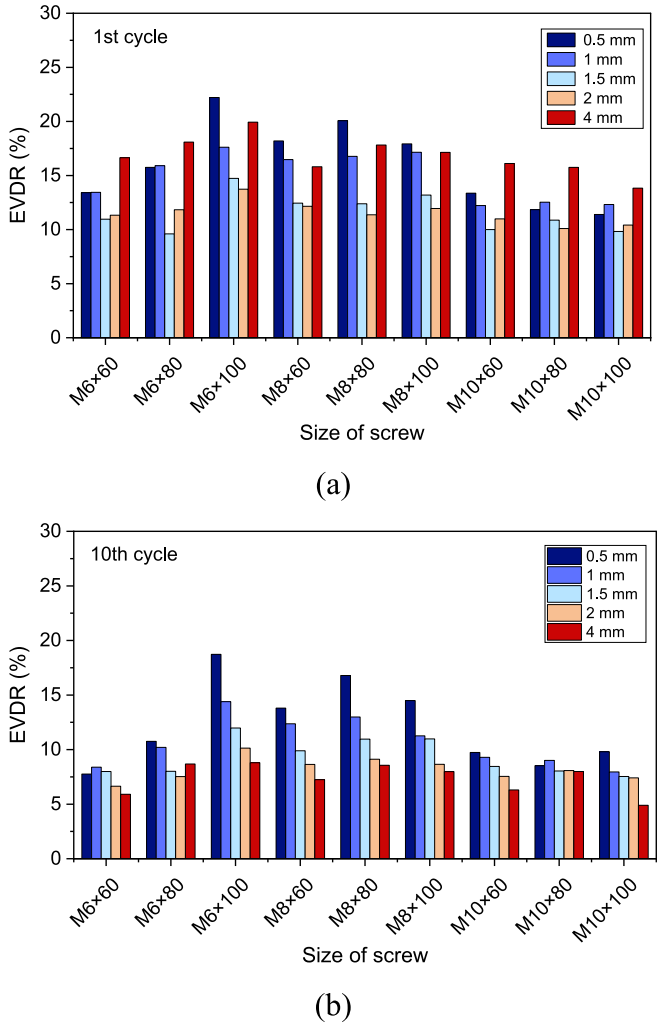

Fig. 9. EVDR of the (a) 1st and (b) 10th cycles at amplitudes of 0.5, 1, 1.5, 2 and 4 mm.

can be explained by referring to the deformation mode depicted in Fig. 6, which exhibits several common characteristics observed in all specimens: 1) The screws did not display noticeable plastic deformation even after undergoing cyclic tests. 2) Triangle-shaped embedment failure of the timber was observed. Consequently, no distinct deformation mode was identified. The presence of these shared characteristics among the specimens resulted in minimal variation in the EVDR across specimens with different screw sizes.

Comparing Fig. 9(a) and (b), the EVDR generally decreased as the number of cycles increased for all specimens. The average EVDRs of the nine analysed specimens in the 1st and 10th circles were 14.2% and 9.6%, respectively. The main reason was that after vibration cycles the CLT around the screws was compressed and did not contribute much in energy dissipation. In addition, it can be found in Fig. 9(a) or (b) that the EVDR for specimens with M6 and M8 screws were slightly higher than that for M10 screws. This may be attributed to the fact that the screws were still slightly deformed, although not significantly. Screws with smaller diameter deformed more and therefore dissipated more energy. In addition, as shown in Fig. 9(a), the EVDR of the 1st cycle at the 4 mm amplitude was generally high, which is consistent with the more evident pinching phenomenon observed in Fig. 7.

2.2.4. *Secant stiffness*

Fig. 10(a) illustrates the maximum load of the beam–panel connection at the 4 mm displacement amplitude. The maximum load increased with the screw diameter, with a distinct linear correlation observed. However, the maximum load was not significantly affected by the screw length. In terms of characterising stiffness degeneration of connections, secant stiffness is a widely used parameter. Fig. 10 (b) shows the secant stiffness of the beam–panel connection. The secant stiffness of the connection increased as the screw diameter increased, and a linear correlation can be found between them. However, no evident relationship was observed between the secant stiffness and screw length.

3. Numerical simulation of the beam–panel connection

In Section 2, the load–displacement behaviour of the screwed beam–panel connection under cyclic loading was obtained. In this section, the load–displacement behaviour of the connection was modelled in OpenSees using zeroLength elements [47] associated with a Pinching4 hysteretic model (Fig. 11). The Pinching4 model can be presented as a piecewise linear curve that shows a pinching load–displacement response, and it can consider the degradation of stiffness and strength under cyclic loading [48]. The model was first proposed by Lowes et al. [44] to simulate the inelastic response of typical beam–column joints of reinforced concrete (RC) frames, and it has been used for bracket connection in CLT shear walls [49] and timber frame RC core hybrid systems [50].

The Pinching4 model uses 16 parameters (ePdi, ePfi, eNdi, eNfi, i = 1,2,3,4) to describe the positive and negative response envelope curves, and 6 parameters (rDispP, rForceP, uForceP, rDispN, rForceN and uForceN) to control the unloading and reloading paths and pinching behaviour. Other parameters control the degradation of unloading stiffness (gK1, gK2, gK3, gK4 and gKLim), reloading stiffness (gD1, gD2, gD3, gD4 and gDLim) and strength (gF1, gF2, gF3, gF4 and gFLim) under cyclic loading. The definition of the parameters can be found in

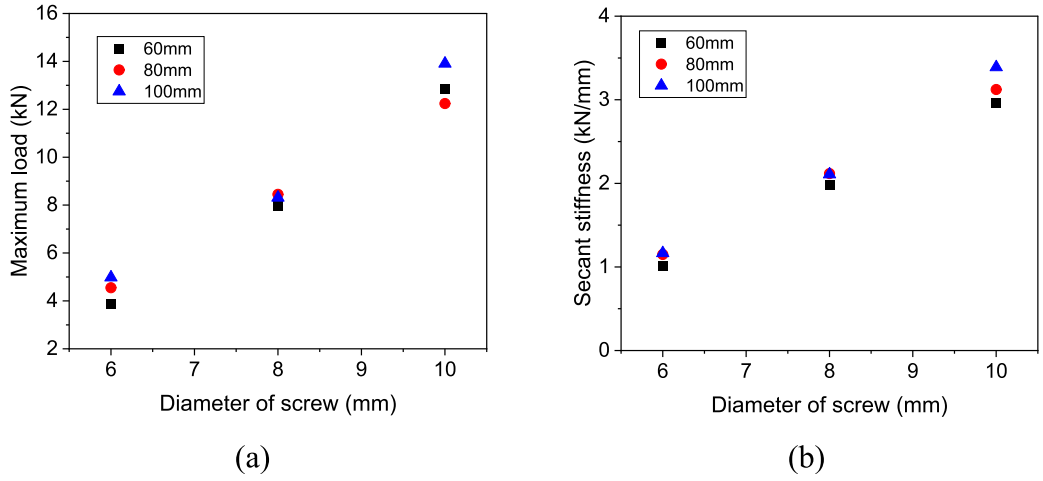

Fig. 10. (a) Maximum load at amplitude of 4 mm; (b) Secant stiffness of the connection.

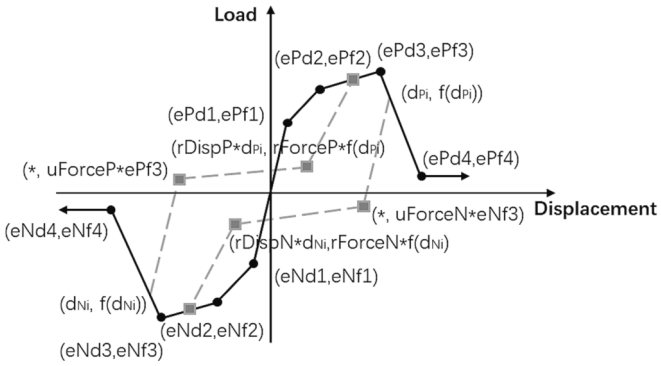

Fig. 11. Load-displacement of Pinching4 model.

[48].

The Pinching4 model parameters were obtained from the load–displacement hysteretic curves. Firstly, the points (ePdi, ePfi) (i = 1,2,3,4) were initially used as an approximation for the envelope of the cyclic test's hysteretic curves for the preliminary fitting process. Specifically, (ePdi, ePfi) (i = 1,2) were identified as the turning points of the loading curve. (ePd3, ePf3) represented the peak load point achieved by monotonically pulling the specimen. As the tests conducted in this study focused on the serviceability state and did not involve failure, the value of (ePd4, ePf4) was estimated and referenced from literature [30]. Subsequently, in order to achieve a more accurate fit to the hysteretic curve (refer to Fig. 7), several modifications were applied to parameters such as (ePdi, ePfi), rDispP, rForceP, uForceP, rDispN, rForceN, uForceN, and gK. These adjustments were implemented to better model the unloading and reloading paths of the hysteretic curves. The Pinching4 model parameters were then used to characterise the beam–panel connection in the numerical model of the full-scale CLT floor. Fig. 12 presents the numerical modelled hysteretic responses for the 60 mm screw connection, demonstrating a good correlation with the experimental curves obtained from cyclic tests.

4. Numerical simulation of the CLT floor under multi-person loading

In Sections 2 and 3, the Pinching4 parameters that characterise the load–displacement behaviour of beam–panel connection were determined. To investigate the influence of coach screw size and spacing on the serviceability of the CLT floor under multi-person loading, a numerical model of the floor was developed in this section, which incorporates the behaviour of the screwed connection.

4.1. Effect of screw size on floor serviceability

4.1.1. Set-up of the numerical model of the floor

Fig. 13(a) shows the tested full-scale CLT floor to be simulated, whose vibration performance has been previously studied [22,51]. The floor dimensions were 6 m length, 5.6 m width and 105 mm thickness (layup: 35L-35 T-35L). Fig. 13(b) illustrates a schematic of the floor. The floor was supported by two HN 450 × 200 steel beams specified in GB/T 11263–2017 [38] and four columns measuring 200 mm × 200 mm × 10 mm that were connected at the bottom to ensure the stability of the

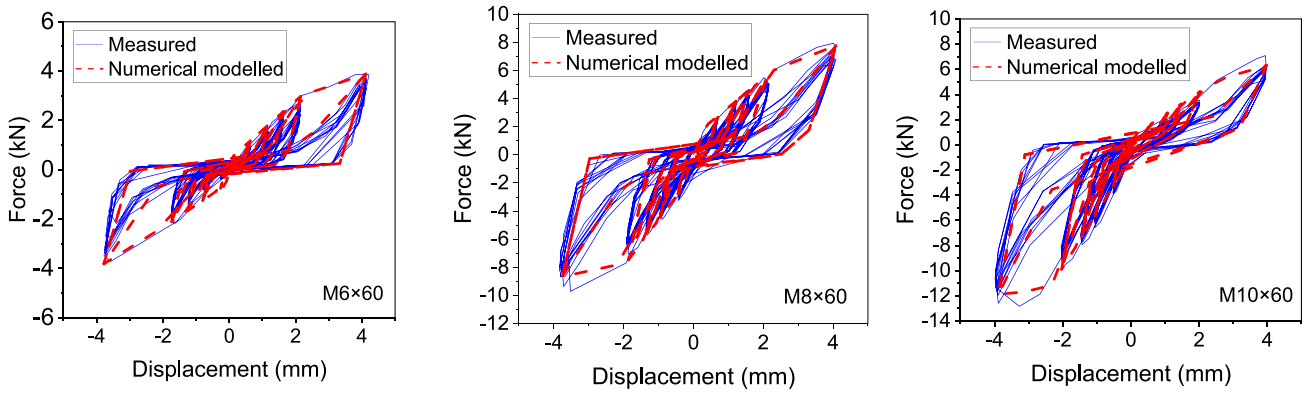

Fig. 12. Comparison of modelled and measured hysteretic response of beam–panel connections for (a) M6 × 60; (b) M8 × 60; (c) M10 × 60.

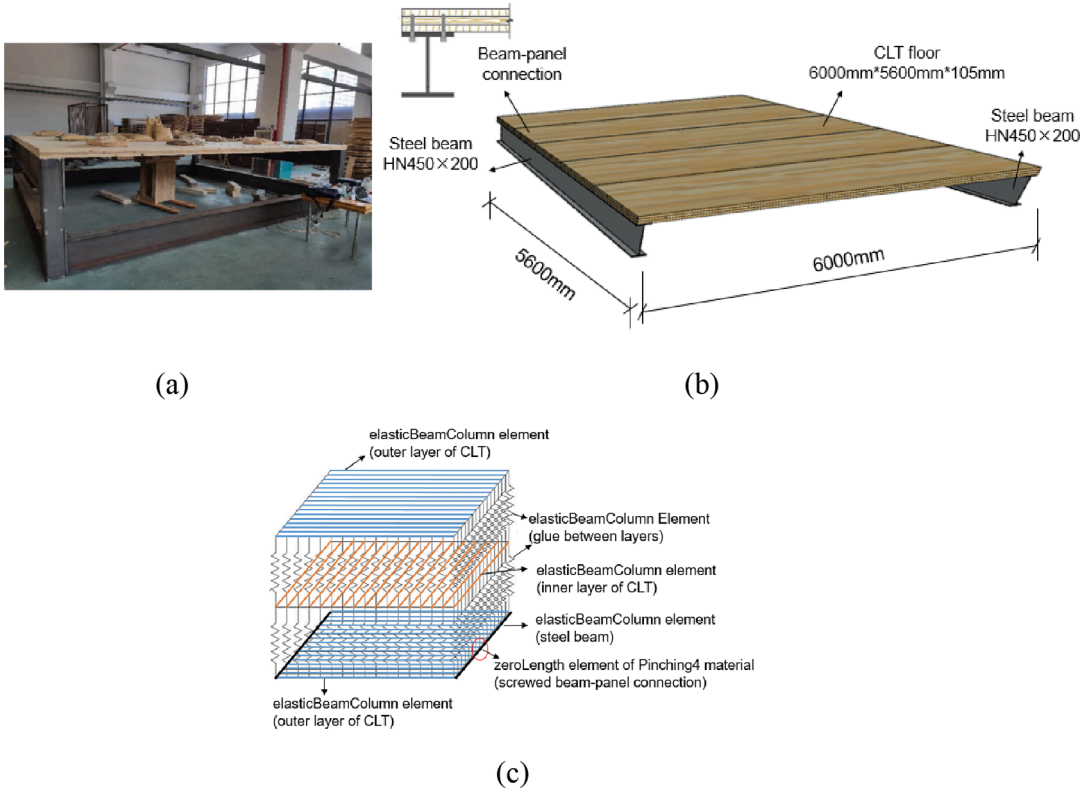

Fig. 13. (a) CLT floor used in laboratory tests [22]; (b) Schematic of the floor; (c) Schematic of the floor modelled in OpenSees [23].

entire floor system. The same CLT used in Section 2 was used for the floor.

The numerical model of the floor was developed in OpenSees, following the authors' previous studies. The validation of the model can be found in the literature [22,23]. Fig. 13(c) shows a schematic of the numerical model, where each layer of the three-ply CLT panel was modelled by a row of elasticBeamColumn elements [52]. The sum of widths of these elements was equal to the overall floor size. The elasticBeamColumn elements in adjacent layers were oriented at 90° to simulate the orthogonal layout of each layer of the CLT panel, as depicted by different colours in Fig. 13(c). The glue connecting the adjacent layers of the CLT panel was simulated by elasticBeamColumn elements, whose stiffness was set to a super large value to prevent any slip between the layers. Compared with previous studies [22,23], the numerical model was improved by considering the load–displacement behaviour of the beam–panel connections, which was simulated by zeroLength elements [47] of the Pinching4 hysteretic model (as discussed in Section 3).

4.1.2. Numerical simulation of human-induced excitation

To perform modal analysis, a heel-drop force was modelled and applied to the central point of the floor. The peak value of this force was set to 70% of the weight of the individual conducting the heel-drop [53]. In this study, the peak value was 0.5 kN, which corresponded to 70% of the weight of a 70 kg person.

As for waking-induced vibration, it's worth noting that the structural responses to multi-person loading differ significantly from those experienced under single-person loading conditions [22]. In daily life, numerous scenarios involve multi-person loading, including situations with multiple family members or colleagues. Therefore, this paper investigates the floor vibration serviceability under multi-person loading. The simulation methodology outlined by Wang et al. [22] was followed. The applied footfall forces simulated the gait of five people crossing the floor in a longitudinal direction and the walking pace was set to be

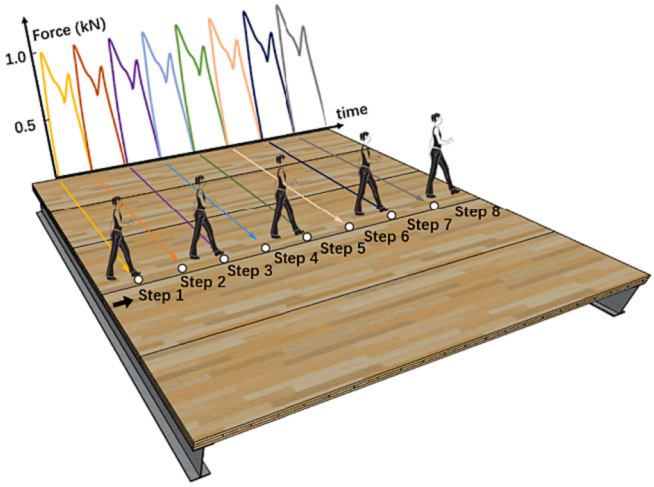

Fig. 14. Schematic of multi-person loading.

1.267 Hz, consistent with previous research [22,51,54]. The time history curve of the footfall force referred to the studies conducted by Galbraith and Barton [55] and Thelandersson and Larsen [56]. The footfall force curves were applied step by step chronologically along the walking path of each person, with the first peak indicating the heel strike and the second peak denoting the toe-off contact. Fig. 14 illustrates the pedestrian excitation.

4.1.3. Numerical results

In Section 4.1, the effect of screw size was investigated while keeping the screw spacing constant. To validate the numerical model, the same screw configuration (M8 × 100 @ 560 mm) as in a previous study [22] was initially used, and screws of different configurations were later used

Table 2
Natural frequencies and damping ratios of the floor.

Size of screws	60 mm			80 mm			100 mm		
	M6	M8	M10	M6	M8	M10	M6	M8	M10
f_1 (Hz)	5.148	5.150	5.151	5.149	5.150	5.151	5.149	5.150	5.152
f_2 (Hz)	7.847	7.853	7.856	7.849	7.853	7.857	7.850	7.853	7.859
Damping ratio (%)	2.05	2.05	2.05	2.04	2.05	2.04	2.04	2.05	2.04

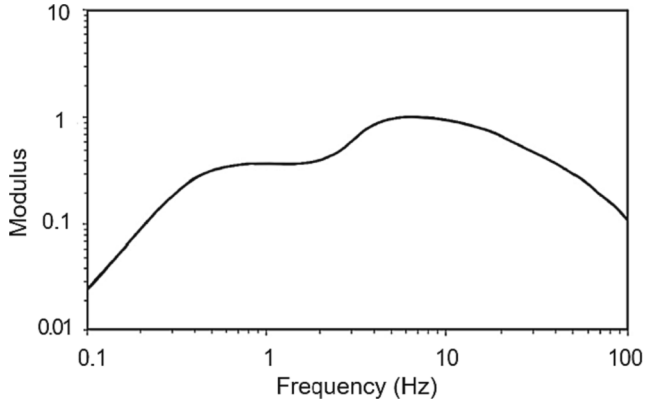

Fig. 15. Frequency weighting curve [8].

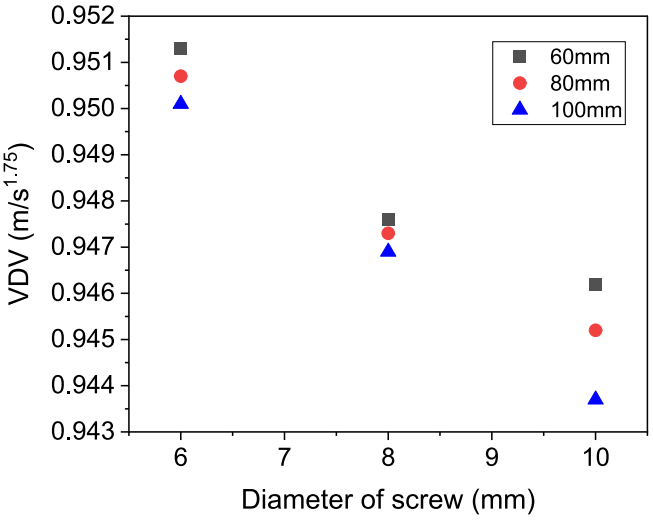

Fig. 16. Relationship between VDV of the floor and diameter of the screw.

on the floor.

The linear-prediction singular-value decomposition-based matrix pencil method [57–59] was used to obtain the fundamental natural frequencies and damping ratios of the floor. The results (Table 2) showed that the fundamental natural frequency of the floor obtained from the numerical simulation was 5.150 Hz, which is close to the experimentally tested value of 5.210 Hz. The fundamental natural frequency of the floor only increased 0.1% as the screw diameter increased, which is practically negligible. The screw length had no obvious effect on the fundamental natural frequency of the floor. The damping ratio of the fundamental frequency mode showed no obvious difference, with an average value of 2.05%. Therefore, the size of screws had limited effect on the dynamic properties of the floor.

The floor vibration serviceability can be evaluated by VDV [10], which can be calculated by Eq. (3):

Table 3
Natural frequencies and damping ratios of the floor.

Spacing between screws (mm)	181	373	560	800	1120	1400
f_1 (Hz)	5.173	5.167	5.150	5.130	5.094	4.960
f_2 (Hz)	7.943	7.916	7.853	7.715	7.739	6.633
Damping ratio (%)	2.05	2.04	2.05	2.04	2.02	2.03

$$VDV = \left(\int_0^T a_w{}^4(t)\mathrm{d}t\right)^{0.25} \tag{3}$$

where the unit of VDV is m/s$^{1.75}$, $a_w(t)$ denotes the frequency-weighted acceleration (in m/s^2), and T represents the total vibration period (in s). The frequency-weighted acceleration $a_w(t)$ in Eq. (3) was obtained by processing the measured acceleration response with a frequency weighting curve (Fig. 15).

The vertical acceleration responses at the central point of the floor under multi-person loading were obtained through numerical simulation, and the VDV for each floor was calculated using Eq. (3) (Fig. 16). Increasing the screw diameter led to a slight decrease of about 1% in the VDV response of the floor. Similarly, the screw length did not show obvious effect on floor serviceability. These findings suggest the limited influence of screw size on the floor vibration serviceability and the minor role of screw size in the overall stiffness of the floor system.

4.2. *Effect of spacing between screws on floor serviceability*

4.2.1. *Numerical model*

In Section 4.2, the effect of spacing between screws on floor serviceability was investigated while keeping the size of screws constant (M8 × 100). In this study, the CLT floor and each steel beam were connected by 32, 16, 11, 8, 6 and 5 pairs of screws, which corresponded to spacing of 181, 373, 560, 800, 1120 and 1400 mm between them, respectively. The spacing was determined based on the floor width and the number of screw pairs. It should be noted that the Austrian National Annex of Eurocode 5 - ÖNORM B 1995–1-1 [60] specifies a maximum screw spacing of 750 mm for CLT-to-steel member connections. However, current prevailing standards do not enforce specific constraints on the maximum screw spacing for CLT-to-steel connection [8,61–65]. Exploring larger screw spacing beyond 800 mm signifies a form of pioneering research. Thoughtfully increasing the screw spacing holds the promise of cost efficiencies in both materials and labour in the construction industry. In the numerical simulation, the same heel-drop and multi-person loading was used as in Section 4.1.

4.2.2. *Numerical results*

The vertical acceleration responses at the central point of the floor under heel-drop excitation and multi-person loading were obtained. Table 3 lists the fundamental natural frequency and damping ratio corresponding to different spacing between screws. When the spacing between screws reduced from 1400 mm to 181 mm, the fundamental natural frequency of the floor increased by 4.3%, which corresponded to an 8.8% increase in the effective stiffness of the floor system. It can be assumed that reducing the spacing between screws increased the stiffness of the beam–panel connection and consequently the effective

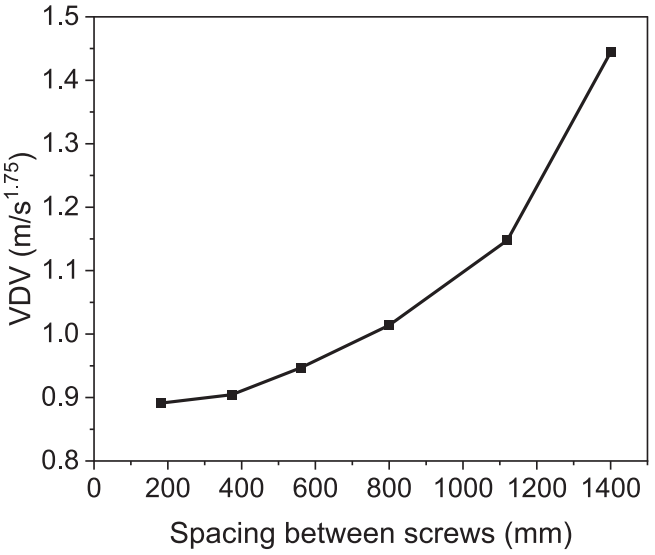

Fig. 17. Relationship between VDV and spacing between screws.

stiffness of the floor system. The damping ratio of the floor did not vary obviously as the spacing between screws decreased (Table 3).

The VDV corresponding to each screw spacing was calculated by Eq. (3) and plotted in Fig. 17. The VDV decreased by 38.3% as the spacing between the screws reduced from 1400 mm to 181 mm, which indicates an improvement in the floor vibration serviceability. As discussed in Section 4.1, increasing the screw diameter resulted in a slight reduction in VDV (1%). Therefore, reduction of spacing between screws is an effective way to improve the floor vibration serviceability during the design process. As illustrated in Fig. 17, an exponential relationship was observed between VDV and screw spacing. An obvious reduction in VDV can be achieved when the screw spacing is large. When the screw spacing is small, its effect on VDV is minimal.

5. Discussion

5.1. Prediction of fundamental natural frequency

To provide a reference for future CLT floor serviceability designs, a theoretical model is proposed to estimate the fundamental natural frequency of a CLT floor system. The floor system investigated in this study consisted of a CLT panel supported on two steel beams connected by coach screws. Theoretically, the fundamental natural frequency of the floor can be calculated using Eq. (4):

Table 4
Theoretical and numerical modelled fundamental natural frequency of the floor (spacing between screws: 560 mm).

Size of screws	Numerical modelled fundamental natural frequencies (Hz)	Predicted fundamental natural frequencies (Hz)	Error (%)
M6 × 60	5.148	5.144	−0.1
M8 × 60	5.150	5.169	0.4
M10 × 60	5.151	5.184	0.6
M6 × 80	5.149	5.144	−0.1
M8 × 80	5.150	5.169	0.4
M10 × 80	5.151	5.184	0.6
M6 × 100	5.149	5.144	−0.1
M8 × 100	5.150	5.169	0.4
M10 × 100	5.152	5.184	0.6

$$f = \frac{1}{2\pi}\sqrt{\frac{k_{\text{eff}}}{m}} \tag{4}$$

where k_{eff} is the effective stiffness of the floor system. In previous study [23], a rigid connection between the floor and supporting beams was assumed. However, the panel was not actually rigidly connected to the beam, and the effect of boundary conditions should be considered to achieve a more accurate design. In this study, the effective stiffness of the floor system k_{eff} is proposed to be considered as a series of the effective bending stiffness of the CLT panel ($k_{\text{CLT panel,eff}}$) and effective stiffness of the boundary condition ($k_{\text{boundary,eff}}$) (Eq. (5)). Each component in Eq. (5) can be calculated by formula, thereby establishing a theoretical framework for predicting the fundamental natural frequency of the floor.

$$k_{\text{eff}} = \frac{1}{\frac{1}{k_{\text{CLT panel,eff}}} + 2 \times \frac{1}{k_{\text{boundary,eff}}}} \tag{5}$$

In Eq. (5) the coefficient 2 denotes that the panel is supported by two steel beams. The $k_{\text{CLTpanel,eff}}$ can be calculated by Eq. (6) [23]:

$$k_{\text{CLTpanel,eff}} = \frac{A_{\text{panel}} \cdot EI_{\text{CLTpanel,eff}} \cdot \left(\frac{\pi}{l_l}\right)^4}{l_t} \tag{6}$$

where l_l and l_t are the longitudinal and transverse length of the CLT floor, respectively. A_{panel} is the area of the CLT panel. $EI_{\text{CLTpanel,eff}}$ can be calculated by Eq. (7) using the shear analogy theory derived from Timoshenko beam theory [23,66]:

$$EI_{\text{CLTpanel,eff}} = \sum_{i=1}^{3} E_i \frac{b_i h_i^3}{12} + \sum_{i=1}^{3} E_i A_i z_i^2 \tag{7}$$

where E_i, b_i, h_i and A_i are the modulus of elasticity, width, height and sectional area of layer i, respectively. z_i denotes the distance between the centroid of the floor section and the centroid of layer i section.

The $k_{\text{boundary,eff}}$ can be regarded as a parallel of the effective torsional stiffness of the steel beam ($k_{\text{beam,eff}}$) and effective shear stiffness of the beam–panel connection ($k_{\text{connection,eff}}$) (Eq. (8)):

$$k_{\text{boundary,eff}} = k_{\text{beam,eff}} + \left(\frac{l_t}{s} + 1\right) \cdot k_{\text{connection,eff}} \tag{8}$$

The $(\frac{l_t}{s}+1)$ corresponds to the number of pairs of screws on each beam, where l_t is the transverse length of the CLT floor and s is the spacing between pairs of screws. The $k_{\text{beam,eff}}$ can be calculated by Eq. (9):

$$k_{\text{beam,eff}} = \frac{8 \cdot G_{\text{beam}} \cdot I_{\text{beam}}}{l_t \cdot l_l \cdot b_{\text{beam}}} \tag{9}$$

where G_{beam} and b_{beam} denote the shear modulus and width of the beam, respectively. I_{beam} is the torsional moment inertia of the steel beam that can be calculated by Eq. (10):

$$I_{\text{beam,eff}} = \frac{2b_{\text{beam}}t_f^3 + (h - 2t_f)t_w^3}{3} \tag{10}$$

where t_f and t_w denote the thickness of the flange and web of the steel beam, respectively.

The $k_{\text{connection,eff}}$ was calculated by Eq. (12). To calculate the elastic stiffness of a screwed connection for the serviceability limit state, Eurocode 5 [8] provides Eq. (11), in which K_{ser} represents the elastic stiffness per shear plane per screw.

$$K_{\text{ser}} = \frac{\rho_m^{1.5} \cdot d}{23} \tag{11}$$

where ρ_m (kg/m^3) is the mean density of CLT, d (mm) is the diameter of the screw.

In this paper, $k_{\text{connection,eff}}$ is equivalent to K_{ser} per shear plane for a

Table 5
Theoretical and numerical modelled fundamental natural frequency of the floor (size of screw: M8 × 100).

Spacing between screws (mm)	Numerical modelled fundamental natural frequencies (Hz)	Predicted fundamental natural frequencies (Hz)	Error (%)
181	5.173	5.218	0.9
373	5.167	5.192	0.5
560	5.150	5.169	0.4
800	5.130	5.141	0.2
1120	5.094	5.108	0.3
1400	4.960	5.082	2.5

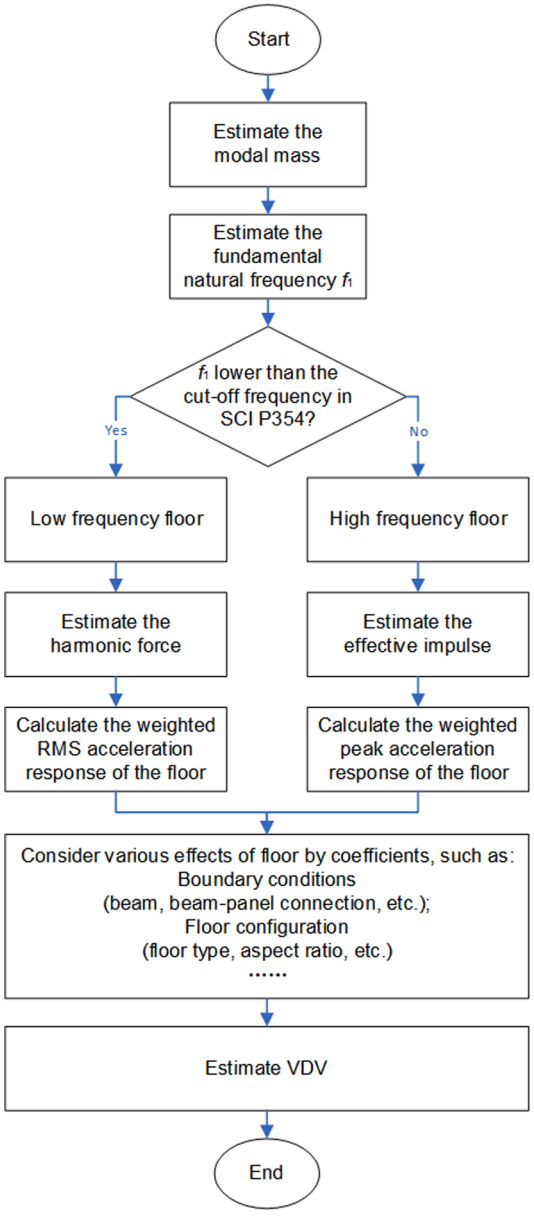

Fig. 18. Proposed method for predicting the VDV of CLT floors.

steel-to-timber connection, as calculated by Eq. (12). In the case discussed in this paper, the connection consists of 2 screws (see Fig. 4), so K_{ser} in Eq. (11) is multiplied by a factor of 2. Additionally, Eurocode 5 [8] specifies that K_{ser} should be multiplied by 2 for steel-to-timber connections. It should be noted that the length of the screw is not considered in this equation for predicting $k_{connection,eff}$ because experimental test results in Section 2.2 indicate that it did not significantly influence the connection stiffness. The calculation for $k_{connection,eff}$ is as follows:

$$k_{connection,eff} = 2 \cdot 2 \cdot K_{ser} = 2 \cdot 2 \cdot \frac{\rho_m^{1.5} \cdot d}{23} \tag{12}$$

Using the theoretical model proposed in this section, the theoretical fundamental natural frequencies of the floor can be estimated based on the dimension and property of the components in the floor system. Tables 4 and 5 show the results of floors with different sizes of screws at a spacing of 560 mm and floors with M8 × 100 screws at different spacing, respectively. The frequencies predicted by the proposed theoretical model correlate well with those obtained from numerical simulations, with an error less than 2.5%, thereby validating the theoretical model.

To sum up, the proposed theoretical model (Eq. (5)) can provide a reference for targeted optimisation of two-side supported CLT floor serviceability design. The stiffness of each component (panel, beam and beam–panel connection) can be calculated, and the floor design can be optimised to improve the vibration serviceability by considering the contribution of each component to the whole floor system. For example, possible improvement methods include changing the tree species or grade of timber materials, changing the size of the supporting beams and modifying the configuration of the fasteners in beam–panel connections.

5.2. Prediction of vibration response

Predicting the response of a floor is crucial in the design process, ensuring a satisfactory vibration performance. In this section, a design method for predicting the vibration serviceability (in terms of VDV) of low-frequency CLT floors is proposed (Fig. 18). This study complements the existing literature [5], which primarily focuses on high-frequency floors, by addressing the case of low-frequency floors. Moreover, the design method proposed in this study takes into account the contribution of steel beam–CLT panel connection, considering the diameter of screws and the spacing between screws, in order to provide more accurate predictions of the VDV for CLT floors.

Specifically, when investigating the human-induced vibration of floors, it is necessary to categorise floors into low-frequency floors and high-frequency floors [11,67]. For low-frequency floors, resonance can lead to severe vibration amplification and steady-state response is primarily investigated. On the other hand, high-frequency floors exhibit greater transient response and require investigation from that perspective. Based on the cut-off frequency defined in SCI P354 [11], the floor studied in this research falls under the category of low-frequency floors. Therefore, a detailed procedure for predicting the VDV of low-frequency floors is presented in this section.

Firstly, the modal mass of the floor is estimated. Literature [68] can be referred to. For the case in this study where two-sided ends of the floor are screwed connected to the supporting beams, the modal mass is conservatively assumed to be 0.5 times of the total mass of the floor [68]. Next, the fundamental natural frequency of the floor is estimated. The method proposed in Section 5.1 can be used, considering the stiffness of the floor panel, the steel beam and the beam–panel connection. Then, the excitation input is estimated. For low-frequency floors, the harmonic dynamic excitation force should be applied. The amplitude of the harmonic force for the h^{th} harmonic, F_h, can be calculated by Eq. (13) according to SCI P354 [11].

$$F_h = \alpha_h G \tag{13}$$

where G is the person's weight (N), h is the order number of the harmonic, α_h is the Fourier coefficient of the h^{th} harmonic. Young [69] proposed the Fourier coefficients α_h for the first four harmonics of footfall force as a function of walking pace which is assumed to be in the range of 1–2.8 Hz. The weighted root-mean-square (RMS) acceleration response can be estimated by Eq. (14), which is modified from SCI P354

Table 6
The VDV obtained by numerical simulation and prediction method.

Spacing between screws (mm)	181	373	560	560	560	800	1120	1400
Diameter of screw (mm)	8	8	6	8	10	8	8	8
Numerical modelled VDV (m/s$^{1.75}$)	0.891	0.905	0.950	0.947	0.944	1.014	1.148	1.445
Predicted VDV (m/s$^{1.75}$)	0.894	0.915	0.951	0.949	0.946	1.012	1.160	1.451

[11].

$$a_{\mathrm{w,RMS},n,h} = \frac{F_h}{M_n\sqrt{2}} D_{n,h} W_{\mathrm{b}} \tag{14}$$

F_h Amplitude of the harmonic force for the h $^{\mathrm{th}}$ harmonic (N), calculated by Eq. (13).

M_n Modal mass of the n $^{\mathrm{th}}$ mode (kg).

$D_{n,h}$ Dynamic magnification factor for acceleration, calculated according to SCI P354 [11].

W_{b} Frequency weighting factor for vertical vibration, see BS 6841 [70] and BS 6472 [10].

When predicting the VDV of high-frequency timber floors, Chang et al. [5] identified a specific relationship between the VDV and weighted peak acceleration calculated by SCI P354 [11]. Referring to this, a method to predict the VDV for low-frequency CLT floors is proposed, in which the first harmonic of the footfall force and the fundamental mode is considered ($a_{\mathrm{w,\,RMS},n=1,h=1}$) for simplicity, as shown in Eq. (15). In Section 4, the VDV for various screw configurations is obtained through numerical simulation. In this section, the weighted RMS acceleration for each screw configuration is computed using theoretical calculation. Consequently, the coefficient 'K' which signifies the relationship between them is obtained. Then, curve fitting is performed based on the coefficient 'K' and the screw configurations (spacing and diameter), and the fitting formula is expressed as Eq. (16). Table 6 shows the VDV obtained by numerical simulation and theoretical prediction, indicating the accuracy of the Eq. (16).

$$VDV \cong K \cdot a_{\mathrm{w,\,RMS},n=1,h=1} \tag{15}$$

$$K = (-0.001d + 1.01)\cdot\left(6e^{s/495} + 183\right) \tag{16}$$

To validate Eq. (15), the theoretical predicted VDV was compared to the experimental VDV in previous experimental study [22]. In [22], the VDV of a cohort of five individuals traversing a full-scale CLT floor at a slow walking pace was recorded as 0.880 m/s$^{1.75}$. In this study, the theoretical prediction method yields a VDV of 0.949 m/s$^{1.75}$. The minor difference between the experimental and theoretical predicted value can be explained by the dissimilarity in the individuals involved. In [22], the VDV was measured for five individuals with different weights, mainly below 70 kg, while in this study, the theoretical prediction is based on an individual weighing 70 kg for a conservative estimation. This distinction in individual characteristics contributes to the observed difference between the experimental and theoretical VDV.

It is important to highlight that in Eq. (15), the weighted RMS acceleration pertains to an individual, while the VDV corresponds to a scenario involving five individuals. Essentially, the coefficient 'K' encapsulates the impact of the number of people involved, and this method has been employed in the study of Wang et al. [22]. In this study, the floor is specifically subjected to a loading condition with five individuals, and Eq. (15) exclusively characterises the VDV under this loading scenario. In other words, this study does not investigate the impact of varying the number of individuals on floor vibration. While it is recognised that there is potential for more intricate equations to predict VDV for different numbers of individuals in the future, exploring this aspect falls outside the scope of this present study.

The idea of relating VDV with $a_{\mathrm{w,\,RMS},n=1,h=1}$ can be used for walking pace in the range of 1–2.8 Hz as specified by Young [69]. It should be noted that various factors such as the dimension of the supporting beam [23], the floor type [54], and the aspect ratio [22] of the floor are beyond the scope of this study and have not been considered here. Future studies will incorporate more factors to provide a more accurate prediction method. It should also be noted that in this paper, the method of predicting VDV by weighted RMS acceleration is proposed for exploratory purposes. Further studies, especially more on-site vibration tests for low-frequency floors, are needed to further validate and improve the method.

6. Conclusion

This study investigated the effect of beam–panel connections on the serviceability of a CLT floor under multi-person loading. Cyclic tests were conducted to obtain the load–displacement behaviour of the beam–panel connections using different screws. A numerical model of a CLT floor was developed to obtain the vibration response of the floor for different screw configurations under multi-person loading. The following conclusions can be drawn:

- The size of screws had limited influence on the fundamental natural frequency and damping ratio of the floor. Reducing the spacing between screws increased the fundamental natural frequency of the floor system by 4.3%, corresponding to an 8.8% increase in the effective stiffness. However, the damping ratio of the floor did not vary obviously.
- Reducing the spacing between screws is an effective way to improve floor serviceability. By varying the screw size among M6/8/10 × 60/80/100, the VDV of the floor only varied about 1%. By reducing the spacing between screws from 1400 mm to 181 mm, the VDV decreased by 38.3%.
- A theoretical model that considered the effective stiffness of the panel, beam and beam–panel connection was proposed to accurately predict the fundamental natural frequency of the CLT floor system, with an error less than 2.5%.
- A design method for predicting the vibration serviceability (in terms of VDV) of low-frequency CLT floors was proposed. The VDV was predicted based on the weighted RMS acceleration response. Various factors, such as the property and boundary conditions of floors, and the human-induced excitation were considered.

The model for predicting the fundamental natural frequency and the design method for predicting the vibration serviceability of CLT floors can be further developed. More measurements, experiments or simulations are needed to fully explore the effects of various factors on the floor vibration serviceability.

CRediT authorship contribution statement

Junhui Zhang: Software, Investigation, Writing – original draft. **Cong Zhang:** Writing – review & editing. **Yi Li:** Supervision, Writing – review & editing. **Wen-Shao Chang:** Conceptualization, Supervision, Writing – review & editing. **Haoyu Huang:** Conceptualization, Methodology, Writing – review & editing, Funding acquisition.

Declaration of Competing Interest

The authors declare that they have no known competing financial interests or personal relationships that could have appeared to influence the work reported in this paper.

Data availability

Data will be made available on request.

Acknowledgement

The authors would like to thank the financial support from Start-Up Funding at Newcastle University and General Project of Science and Technology Plan of Beijing Municipal Education Commission [Grant No. KM202310005022].

References

[1] Liang S, Gu H, Bergman R. Environmental life-cycle assessment and life-cycle cost analysis of a high-rise mass timber building: a case study in pacific Northwestern United States. Sustain 2021:7831–47. https://doi.org/10.3390/su13147831.
[2] United Nations Department of Global Communications. Sustainable Development Goals. 2020. (Access date: 7th April 2023). https://www.un.org/en/desa/sustainable-development-goals-report-2020.
[3] Brandt K, Gold K, Harty M, Taggart J, Turner M, Wylie D. Naturally Wood British Columbia. Canada: Naturally Wood; 2019.
[4] WoodWorks. Market Trends Map. Snapshot of Mass Timber Projects in Design, Under Construction and Built in the U.S. (Access date: 7th April 2023), https://www.woodworks.org/resources/mapping-mass-timber/.
[5] Chang WS, Goldsmith T, Harris R. A New Design Method for Timber Floors – Peak Acceleration Approach. In: International Network on Timber Engineering Research. Tallinn, Estonia: Timber Scientific; 2018. p429–44.
[6] Huang H, Zhang J, Uttley J, Chang WS, Wang BJ. The Effect of the Environment on the Serviceability of the Cross-Laminated Timber (CLT) Floor: Virtual Reality as a Research Tool. Adv Civ Eng 2022:7562656. Doi: 10.1155/2022/7562656.
[7] Feldmann M, Heinemeyer C, Butz C, Caetano E, Cunha A, Galanti F, et al. Design of floor structures for human induced vibrations. JRC Report. 2009 https://eurocodes.jrc.ec.europa.eu/publications/design-floor-structures-human-induced-vibrations.
[8] EN 1995-1-1:2004+A2:2014. Eurocode 5: Design of timber structures — Part 1-1: General — Common rules and rules for buildings. Brussels: European Committee for Standardization; 2014.
[9] Iso 10137:2007.. Bases for design of structures — Serviceability of buildings and walkways against vibrations. Geneva: International Organization for Standardization; 2007.
[10] Bs 6472–1:2008.. Guide to evaluation of human exposure to vibration in buildings — Part 1: Vibration sources other than blasting. London: British Standards Institution; 2008.
[11] Smith AL, J hs, j dp.. Design of Floors for Vibration: A New Approach (SCI Publication P354). Berkshire: The Steel Construction Institute (SCI) 2009.
[12] Murray TM, Allen DE, Ungar EE. Floor vibrations due to human activity. AISC/CISC Steel Design Guide Series 11. US: American Institute of Steel Construction 1997.
[13] Willford MR, Young P. A design guide for footfall induced vibration of structures (CCIP-016). Trowbridge, UK: The Concrete Centre; 2006.
[14] Ellingwood B, Tallin A. Structural Serviceability: Floor Vibrations. J Struct Eng 1984;110:401–18.
[15] Smith I, Chui YH. Design of lightweight wooden floors to avoid human discomfort. Can J Civil Eng 1988;15:254–62.
[16] Al-Foqaha'a AA, Cofer WF, Fridley KJ. Vibration Design Criterion for Wood Floors Exposed to Normal Human Activities. J Struct Eng 1999;125:1401–6.
[17] Onysko DM, Hu L, Jones EL, Lenardo BD. Serviceability design of residential wood-frame floors in Canada. In: World Conference on Timber Engineering (WCTE); 2000. p. 1–8.
[18] Hu L, Chui YH, Onysko DM. Vibration serviceability of timber floors in residential construction. Prog Struct Eng Mater 2001;3:228–37. https://doi.org/10.1002/pse.69.
[19] Hu L, Chui YH. Development of a Design Method to Control Vibrations Induced by Normal Walking Action in Wood-Based Floors. In: World Conference on Timber Engineering (WCTE); 2004. p. 1–6.
[20] Hamm P, Richter A, Winter S. Floor vibrations – new results. In: World Conference on Timber Engineering (WCTE); 2010. p. 1–10.
[21] Weckendorf J, Toratti T, Smith I, Tannert T. Vibration serviceability performance of timber floors. Eur J Wood Wood Prod 2016;74:353–67. https://doi.org/10.1007/s00107-015-0976-z.
[22] Wang C, Chang WS, Yan W, Huang H. Predicting the human-induced vibration of cross laminated timber floor under multi-person loadings. Structures 2021;29:65–78. https://doi.org/10.1016/j.istruc.2020.10.074.
[23] Huang H, Gao Y, Chang WS. Human-induced vibration of cross-laminated timber (CLT) floor under different boundary conditions. Eng Struct 2020;204:110016. https://doi.org/10.1016/j.engstruct.2019.110016.
[24] Jarnerö K, Brandt A, Olsson A. Vibration properties of a timber floor assessed in laboratory and during construction. Eng Struct 2015;82:44–54. https://doi.org/10.1016/j.engstruct.2014.10.019.
[25] Shahnewaz M, Dickof C, Zhou J, Tannert T. Vibration and flexural performance of cross-laminated timber – glulam composite floors. Compos Struct 2022;292:115682. https://doi.org/10.1016/j.compstruct.2022.115682.
[26] Asiz A, Smith I. Demands placed on steel frameworks of tall buildings having reinforced concrete or massive wood horizontal slabs. Struct Eng Int 2009;19:395–403. https://doi.org/10.2749/101686609789847000.
[27] Asiz A, Smith I. Connection system of massive timber elements used in horizontal slabs of hybrid tall buildings. J Struct Eng 2011;137:1390–3. https://doi.org/10.1061/(ASCE)ST.1943-541X.0000363.
[28] Loss C, Piazza M, Zandonini R. Connections for steel–timber hybrid prefabricated buildings. Part I: Experimental tests. Constr Build Mater 2016;122:781–95. https://doi.org/10.1016/j.conbuildmat.2015.12.002.
[29] Elliottwood. 92-120 Notting Hill Gate, London. (Access date: 15th July 2023), https://www.elliottwood.co.uk/projects/92-120-notting-hill-gate-london.
[30] Ataei A, Chiniforush AA, Bradford MA, Valipour H. Cyclic behaviour of bolt and screw shear connectors in steel-timber composite (STC) beams. J Constr Steel Res 2019;161:328–40. https://doi.org/10.1016/j.jcsr.2019.05.048.
[31] He M, Li M, Li Z, He G, Sun Y. Mechanical performance of glulam beam-to-column connections with coach screws as fasteners. Arch Civ Mech Eng 2021;21:51–68. https://doi.org/10.1007/s43452-021-00207-5.
[32] Hassanieh A, Valipour HR, Bradford MA. Experimental and numerical investigation of short-term behaviour of CLT-steel composite beams. Eng Struct 2017;144:43–57. https://doi.org/10.1016/j.engstruct.2017.04.052.
[33] Hassanieh A, Valipour HR, Bradford MA. Load-slip behaviour of steel-cross laminated timber (CLT) composite connections. J Constr Steel Res 2016;122:110–21. https://doi.org/10.1016/j.jcsr.2016.03.008.
[34] Hassanieh A, Valipour HR, Bradford MA. Composite connections between CLT slab and steel beam: Experiments and empirical models. J Constr Steel Res 2017;138:823–36. https://doi.org/10.1016/j.jcsr.2017.09.002.
[35] Hassanieh A, Valipour HR, Bradford MA. Experimental and analytical behaviour of steel-timber composite connections. Constr Build Mater 2016;118:63–75. https://doi.org/10.1016/j.conbuildmat.2016.05.052.
[36] Chiniforush AA, Makki Alamdari M, Dackermann U, Valipour HR, Akbarnezhad A. Vibration behaviour of steel-timber composite floors, part (1): Experimental & numerical investigation. J Constr Steel Res 2019;161:244–57. https://doi.org/10.1016/j.jcsr.2019.07.007.
[37] Hassanieh A, Chiniforush AA, Valipour HR, Bradford MA. Vibration behaviour of steel-timber composite floors, part (2): Evaluation of human-induced vibrations. J Constr Steel Res 2019;158:156–70. https://doi.org/10.1016/j.jcsr.2019.03.026.
[38] GB/T 11263-2017. Hot-rolled H and cut T section steel. Beijing: Standards Press of China; 2017. [in Chinese].
[39] GB/T 700-2006. Carbon structural steels. Beijing: Standards Press of China; 2006. [in Chinese].
[40] Din. 571. Hexagon head wood screws. Germany: German Institute for Standardization; 2016.
[41] Huang H, Chang WS. Seismic resilience timber connection—adoption of shape memory alloy tubes as dowels. Struct Control Health Monit 2017;24:e1980.
[42] En BS, 12512:2001.. Timber structures - Test methods - Cyclic testing of joints made with mechanical fasteners. London: British Standards Institution; 2001.
[43] Hossain A, Popovski M, Tannert T. Cross-laminated timber connections assembled with a combination of screws in withdrawal and screws in shear. Eng Struct 2018;168:1–11. https://doi.org/10.1016/j.engstruct.2018.04.052.s.
[44] Lowes LN, Mitra N., Altoontash A. A Beam-Column Joint Model for Simulating the Earthquake Response of Reinforced Concrete Frames. PEER Report 2003-10. Pacific Earthquake Engineering Research Center, University of California, Berkeley, CA.
[45] Leijten AJ, Ruxton S, Prion H, Lam F. Reversed-Cyclic Behavior of a Novel Heavy Timber Tube Connection. J Struct Eng 2006;132(8):1314–9. https://doi.org/10.1061/(ASCE)0733-9445(2006)132:8(1314).
[46] Popovski M, Prion HGL, Karacabeyli E. Seismic performance of connections in heavy timber construction. Can J Civil Eng 2002;29:389–99. https://doi.org/10.1139/L02-020.
[47] Fenves GL. ZeroLength Element (OpenSees User Documetation). 2014. (Access date: 7th April 2023). https://opensees.berkeley.edu/wiki/index.php/ZeroLength_Element.
[48] Mitra N. Pinching4 Material (OpenSees User Documetation). 2012. (Access date: 7th April 2023). https://opensees.berkeley.edu/wiki/index.php/Pinching4_Material.
[49] Shen YL, Schneider J, Tesfamariam S, Stiemer SF, Mu Z-G. Hysteresis behavior of bracket connection in cross-laminated-timber shear walls. Constr Build Mater 2013;48:980–91. https://doi.org/10.1016/J.CONBUILDMAT.2013.07.050.
[50] Isoda H, Tesfamariam S. Connections for Timber-Concrete Hybrid Building: Experimental and Numerical Model Results. J Perform Constr Facil 2016;30:04016024. https://doi.org/10.1061/(ASCE)CF.1943-5509.0000849.
[51] Huang H, Wang C, Chang WS. Reducing human-induced vibration of cross-laminated timber floor—Application of multi-tuned mass damper system. Struct Control Health Monit 2021;28:e2656.
[52] fmk. Elastic Beam Column Element (OpenSees User Documetation). 2023. (Access date: 7th April 2023). https://opensees.berkeley.edu/wiki/index.php/Elastic_Beam_Column_Element.
[53] Glišović I, Stevanović B. Vibrational behaviour of timber floors. In: World Conference on Timber Engineering (WCTE); 2010. p. 1–10.
[54] Huang H, Lin X, Zhang J, Wu Z, Wang C, Wang BJ. Performance of the hollow-core cross-laminated timber (HC-CLT) floor under human-induced vibration. Structures 2021;32:1481–91. https://doi.org/10.1016/j.istruc.2021.03.101.
[55] Galbraith F, Barton M. Ground Loading from Footsteps. J Acoust Soc Am 1970;48:1288–92. https://doi.org/10.1121/1.1912271.
[56] Thelandersson S, Larsen H. Timber Engineering. Chichester: Wiley; 2003. p. 446.

[57] Hua Y, Sarkar TK. Matrix pencil method for estimating parameters of exponentially damped/undamped sinusoids in noise. IEEE Trans Acoust. Speech Signal Process 1990;38(5):814–24. https://doi.org/10.1109/29.56027.
[58] Zieliński TP, Duda K. Frequency and damping estimation methods - an overview. Metrol Meas Syst 2011;18:505–28. https://doi.org/10.2478/v10178-011-0051-y.
[59] Sarkar TK, Pereira O. Using the matrix pencil method to estimate the parameters of a sum of complex exponentials. IEEE Antennas Propag Mag 1995;37(1):48–55. https://doi.org/10.1109/74.370583.
[60] ÖNORM B 1995-1-1. Eurocode 5: Design of timber structures - Part 1-1: General - Common rules and rules for buildings - Consolidated version with national specifications, national comments and national supplements for the implementation of ÖNORM EN 1995-1-1. Vienna: Austrian Standards International; 2015.
[61] Gustafsson A, The CLT, Handbook.. CLT structures — facts and planning. Floor structures. First edition. Stockholm: Swedish Wood 2019:90–109.
[62] Wurth. Cross-laminated timber connections: Wall and floor assemblies, p.1-16.
[63] Karacabeyli E, Gagnon S. Canadian CLT Handbook. 2019 edition. Pointe-Claire: FPInnovation; 2019. p. 1–832.
[64] Council AW, Specification ND, (NDS) for Wood Construction,. Edition. Leesburg, US: American Wood Council 2018;2018:1–206.
[65] Trada. TRADA cross-laminated timber series. TRADA 2009:1–84.
[66] Christovasilis IP, Brunetti M, Follesa M, Nocetti M, Vassallo D. Evaluation of the mechanical properties of cross laminated timber with elementary beam theories. Constr Build Mater 2016;122:202–13. https://doi.org/10.1016/j.conbuildmat.2016.06.082.
[67] Nguyen HAT. Vibrations of a low-frequency floor under various pedestrian loading scenarios. Arch Civil Eng Environ 2021;14:105–14. https://doi.org/10.21307/ACEE-2021-034.
[68] Kollár LP, Pap ZB. Modal mass of floors supported by beams. Structures. 2018;13:119–30. https://doi.org/10.1016/j.istruc.2017.12.002.
[69] Young P. Improved floor vibration prediction methodologies. Arup Vibration Seminar on Engineering for Structural Vibration — Current Developments in Research and Practice. London, UK: 2001.
[70] BS 6841:1987. Guide to measurement and evaluation of human exposure to whole-body mechanical vibration and repeated shock. London: British Standards Institution; 1987.